Susceptibility and Relaxation Tensor Properties of Multiple Sclerosis Lesions at 3T

Cynthia Wisnieff[1], Alexey Dimov[1,2], David Pitt[3], and Yi Wang[1,2]

[1]*Biomedical Engineering, Cornell University, Ithaca, New York, United States,* [2]*Radiology, Weill Cornell Medical College, New York, New York, United States,* [3]*Neurology, Yale University, New Haven, Connecticut, United States*

Target Audience: Researchers and clinicians interested in susceptibility and relaxation tensor properties of multiple sclerosis lesions

Introduction:

Changes in the structure of the myelin sheath is a key feature of the pathogenic process of demyelination in multiple sclerosis (MS) lesions. Recent studies of the susceptibility and relaxation properties of tissue have demonstrated their sensitivity to both the structure and molecular order of myelin of white matter (WM). In this work we investigate changes in the susceptibility and relaxation tensor properties that have occurred in WM lesions of ex vivo MS brain specimens.

Methods:

MRI acquisition: A total of 7 formalin fixed MS brain specimens were imbedded in 1% agar for imaging. A multiple echo acquisition was performed on a GE 3T MR750 for each of 16 unique orientations of the phantom evenly distributed in space. Oblique planes following the phantom were used to reduce acquisition time and improve the post-acquisition image registration. Imaging parameters were TR/TE spacing/#Echoes: 53.8ms/ 4.15ms/12 echoes at a resolution of 0.75x0.75x0.8mm^3.

Image Analysis: A susceptibility tensor imaging (STI) was reconstructed by solving the field to source inversion problem using a conjugate gradient method. Relaxation tensor imaging (R2*T) was computed from a fit of a rank 2 tensor to the apparent relaxation rate observed in each orientation from a log-transformed linear fit of the echoes. The anisotropy A was calculated as the major difference in principal eigenvalues, $= \lambda_1 - \lambda_3$, both for R2*T (denoted by R2*A) and for STI (denoted by MSA). Here, the λ_is are the eigenvalues sorted in decreasing order. Alignment between principle eigenvectors was calculated as $|\boldsymbol{V}_{\boldsymbol{\chi}} \cdot \boldsymbol{V}_{\boldsymbol{R}_2^*}|$, where $\boldsymbol{V}_{\boldsymbol{\chi}}$ and $\boldsymbol{V}_{\boldsymbol{R}_2^*}$ are the principal eigenvectors from STI and R2*T, respectively. The mean susceptibility/relaxation value of a susceptibility/relaxation tensor $\boldsymbol{T}$ was calculated as $\overline{\boldsymbol{T}} = (\lambda_1 + \lambda_2 + \lambda_3)/3$. Measurements of tensor properties and alignment where made in ROIs of the 5 largest WM lesions and the Corpus Callosum when present on the specimen.

Results:

Figure 1 shows an example of estimated STI and R2*T tensor maps. The bottom row displays the mean susceptibility/relaxation tensor properties from STI and R2*T compared to standard wT2 imaging, showing changes in both the MS lesions indicated by the arrows and normal appearing corpus callosum (CC). The orientation of CC between STI and R2*T appears in the first column of Table 1, showing reduction of alignment ($|\boldsymbol{V}_{\boldsymbol{\chi}} \cdot \boldsymbol{V}_{\boldsymbol{R}_2^*}|$), MSA and R2*A, and increase of $\bar{\chi}$ and decrease of R2* in MS lesions compared to CC.

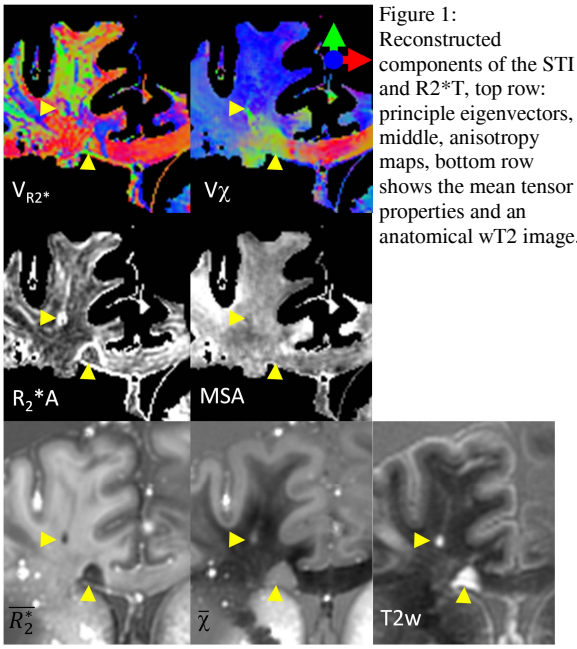

Figure 1: Reconstructed components of the STI and R2*T, top row: principle eigenvectors, middle, anisotropy maps, bottom row shows the mean tensor properties and an anatomical wT2 image.

Table 1: Measured ROIs in WM lesions and NAWM.

		$\lvert\boldsymbol{V}_{\boldsymbol{\chi}} \cdot \boldsymbol{V}_{\boldsymbol{R}_2^*}\rvert$	MSA	R_2*A	$\bar{\chi}$	$\overline{R_2^*}$
Lesion	1	0.39±0.25	15±3	2.2±0.69	26.8±2.2	7.3±0.91
	2	0.46±0.30	23±2	3.0±2.3	6.5±1.2	7.2±1.81
	3	0.37±0.22	37±3	1.4±0.57	8.3±2.7	4.9±0.72
	4	0.41±0.22	35±3	1.3±0.35	-1.7±0.9	7.3±0.65
	5	0.48±0.32	34±3	2.5±0.96	6.6±4.3	9.4±2.98
Corpus Callosum	1	0.60±0.14	38±8	3.2±0.88	-37.1±2.5	19.1±0.51
	2	0.72±0.24	50±20	2.9±0.62	-57.6±4.1	22.7±0.54

Discussion:

The first row of Fig. 1 and column of Table 1 show that the alignment of the corpus callosum, a major white matter tract agrees well between both tensors (>0.60) and there is a decrease in alignment within the lesions measured (<0.50). This is consistent with the demyelination of lesions in multiple sclerosis where the myelin, the major contributor to the anisotropy of the tissue, is disrupted. There are some difficulties in examining the more peripheral normal appearing white matter as it is difficult to disentangle the contribution from crossing fibers in healthy white matter and demyelination in normal appearing white matter to the isotropy of the tensor properties. From the bottom row of Figure 1 the mean relaxation R2* and susceptibility $\bar{\chi}$ properties yield good image quality: while R2* cannot differentiate demyelination from iron deposit, lesions with $\bar{\chi}$>0 must have paramagnetic iron, as demyelination alone can only increase $\bar{\chi}$ to zero.

The anisotropy measures suffer from increased noise from the computation of the difference of eigenvalues. There is an artifact in the reconstructed R2*T where the boundaries between two regions with significantly different relaxation properties suffer from differing partial volume effects from each orientation, which artificially increases the anisotropy of the border. This preliminary data is promising in investigating changes in the susceptibility and relaxation properties of WM from changes in tissue structure in MS lesions.

Conclusion:

Magnetic tenor property changes in MS lesion may be studied using quantitative susceptibility tensor and R2* tensor in MRI

References: 1.Hametner, S., et al., Ann Neurol, 2013.2.Pitt, D., et al., Arch Neurol, 2010. **67**(7): p. 812-8. 3.Mehta, V., et al., PLoS One, 2013. **8**(3): p. e57573. 4.Liu, T., et al., MRM, 2009. **61**: p. 196-204. 5. Liu, C., MRM, 2010. **63**(6): p. 1471-7. 6.Jenkinson, M. and S. Smith. Med Image Anal, 2001. **5**(2): p. 143-56. 7. Jenkinson, M., et al., Neuroimage, 2002. **17**(2): p. 825-41. 8.Langkammer, C., et al., Neuroimage, 2012. **62**(3): p. 1593-9.